VARIATION AND ANISOTROPY OF REFLECTANCE OF FOREST TREES IN RADIOMETRICALLY CALIBRATED AIRBORNE LINE SENSOR IMAGES – IMPLICATIONS TO SPECIES CLASSIFICATION

I. Korpela *, F. Rohrbach

Faculty of Agriculture and Forestry, University of Helsinki, POB 27, 00014 UH, Finland - (ilkka.korpela@helsinki.fi)

Commission VII

KEY WORDS: Forestry, Radiometry, Modelling, Calibration, Pushbroom, Multispectral, LiDAR,

ABSTRACT:

In Scandinavia, the conventional method of measuring trees is giving way to applications, which combine *in-situ* and airborne optical data, LiDAR in particular. Tree species (sp.) classification is a crucial sub-task and is solved with an insufficient reliability. The continuously varying view-illumination geometry hampers image-based solutions. Line sensors provide a selected subset of the possible view-illumination geometries, but have not been tried for the task in Scandinavia. We examined the variation and anisotropy of reflectance in trees, using radiometrically calibrated multispectral ADS40 data. An experiment in Finland (61°50'N, 24°20'E) that consisted of 121 plots and 15197 pine, spruce, and birch trees was imaged from 1, 2, 3, and 4 km altitudes. Leica XPro was used for producing different image data including the at-sensor radiance (ASR) data, atmospherically (ATM) corrected, and a combined BRDF- and atmospheric correction (FULL). Tree crowns were modelled in LiDAR data, and the resulting envelopes were sampled in the images in 121 points. Using the geometry of the crown envelope and the adjacent LiDAR points to model the geometry of the neighbourhood, camera-visibility and illumination class (Sun-lit, self-shaded, neighbour-shaded) was determined for each point. Using the pixel data of the crown points, different statistical features were derived for each tree. The radiometrically corrected image data did not reduce the intraspecies coefficient of variation, and in sp. classification trials, the ASR data provided equal or better results. The precision of the ATM data was evaluated to be better than 10% with the NIR band being most precise and the BLU band least precise. However, the BLU band was a strong predictor of tree species. Reflectance anisotropy of pine and spruce differed from birch, and it was strongest in the visible bands and varied up to ± 40% in nadir lines flown nearly perpendicular to the Sun. Reflectance of crowns in diffuse illumination showed lower anisotropy and features derived in these data were strong predictors of species. We observed notable proximity effects in the NIR band, where the species composition of the adjacent trees affected the observed reflectance of the target tree up to 33%. Intracrown reflectance variation was examined for crown points oriented towards or away from the Sun on different relative heights. Age dependencies were observed in NIR and NDVI, where age explained up to 5% of the reflectance variation, and the dependency was negative. Site fertility was correlated with NIR and NDVI, and the overall stand effect explained 1–19% of the reflectance variation by band and species. This elucidates, why also the tree species classification accuracy varied considerably between stands. Classification accuracy for pine, spruce, and birch was 72–80% in quadratic discriminant analysis, when features of both Sun-lit and diffuse light were used as predictors. Best-case accuracies of 76–80% were achieved using 3 and 4 km monoscopic data, which shows the high potential of the ADS40 line sensor.

1. INTRODUCTION

In Scandinavia, the conventional method of measuring trees is giving way to applications, which combine *in-situ* and RS data. Here, the introduction of airborne LiDAR was a breakthrough. The need for aerial images is a topical question amongst Scandinavian foresters to whom species information is crucial on technical, economic, and ecological grounds. Separation of Scots pine, Norway spruce, and birch is essential for forestry in Finland. Classification accuracies of above 90% are considered adequate for practice. Recently, low-altitude, high-density discrete-return LiDAR data were tested for tree species discrimination with accuracies saturating at the 85–90% level. Owing to the monostatic view-illumination configuration, LiDAR signal is largely free from view-angle effects that have been reported to hamper image-based tree species recognition. In Sweden, an accuracy of 84% was reported in 1 km altitude, digital frame camera data (60 cm GSD DMC) (Holmgren et al 2008).

The validation procedures used for estimating species classification accuracy should provide realistic demonstrations of the performance. The leave-one-out cross-validation is often used. It results in optimistic evaluation of the performance, omitting the spatial autocorrelation in forests and the similarity of view-illumination effects for neighbouring trees.

A species classification accuracy of 95% would be adequate for foresters in Finland, which is very challenging in airborne optical data, because the observations from the above result in commission and omission errors in tree detection. If a small tree is detected in near-nadir LiDAR, the low solar elevation, <53° in Finland, prevents from observing but the tallest trees in direct light. Species identification in image-based analysis is hampered by the view-illumination geometry (Fig. 1). According to Li and Strahler (1986), the geometric nature of the forest canopy is the major factor explaining the strong anisotropy of directional reflectance. Anisotropy of the reflectance is a fundamental property of most objects, and it means that the observed brightness is dependent on the illumination and observation directions. For point-like illumination and observer, the dependence can be described by the BRDF, depending on two illumination and two observation angles. Illumination conditions in forest canopy range from direct illumination to combinations of diffuse and direct illumination down to the total diffuse illumination,

* Corresponding author

with different levels of adjacent illumination sources. For those conditions various other reflectance quantities are needed (Martonchik et al., 2000).

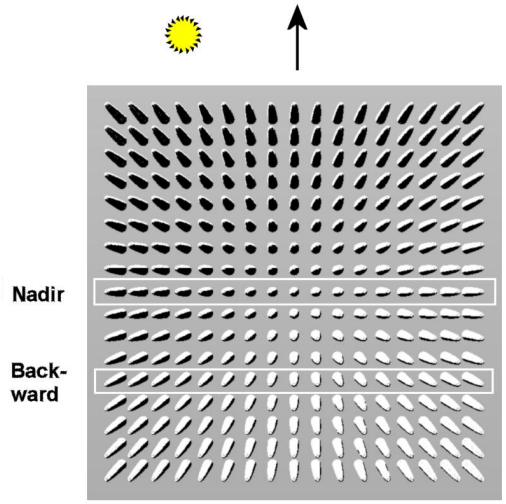

Figure 1. Illustration of the view-illumination geometry of trees in the focal plane of a nadir looking aerial camera. The flying direction is upwards and Sun is 26° left of it. The white rectangles depict the nadir and backward viewing in the ADS40 line sensor, which we used in this study.

Depending on the view and illumination directions, the pixel can view, in the extreme case of hot-spot geometry, shadow-free targets. When a tree crown is back-lit, the pixels sample mostly shadowed targets or forward-scattering canopy elements. The diffuse light incident at a tree consists of the light scattering in the atmosphere, but also of light scattered by the adjacent trees and the background. Taller neighboring trees are both reflectors that contribute to the incident light, but they also attenuate hemispherical diffuse light. Multiple scattering by trees contributes to the total radiance towards the sensor.

The spectra of a tree in an aerial image are measured from a sample of pixels that are geometrically linked to the tree. If the geometry of the canopy is known, it is possible to sample the crown for the Sun-lit and shaded parts (Korpela, 2004; Larsen 2007)..

There are many sources of inter- and intratree reflectance variation. The varying phenological and physiological status affects reflectance. Epiphytic lichens, flowers, and cones constitute sources of variation. The structure of branches, shoots, and needles, and the whole branching pattern and crown shape vary between and inside individuals, and the crown structure changes with age. The functioning, structure, and the environment all interrelate in a tree. Structural differences explain largely the variation in reflectance and anisotropy.

The scale of observation has important implications. In aerial images, a crown can be sampled by hundreds of pixels, while in satellite images several crowns fill a pixel. In sub-meter pixels, the scale is at the level of branches and shoots. Since bidirectional effects have their origin in sub-pixel shadow casting, it is possible to observe branch-level anisotropy. Scale is linked with sensor altitude and the medium. The majority of the atmospheric effects occur below the 3–6 km altitude, which stresses the importance of atmospheric modeling in airborne images if target reflectance data is strived for.

The introduction of digital sensors, direct sensor orientation, and image post processing systems, have all altered photogrammetric practices. In forest applications, this development has been covered by the expansion of LiDAR. Digital sensors are relatively calibrated to a uniform response or absolutely calibrated to produce at-sensor radiance (ASR) data. Among photogrammetric sensors, absolute calibration exists for the ADS40 line camera. It measures ASR in 4 bands in two directions. A laboratory calibration is applied throughout a radiometry chain that also includes radiometric correction methods, which are implemented in the Leica XPro software (Beisl et al., 2008). The performance of ADS40 in tree species classification in Finland was simulated in Heikkinen et al. (2010). An additional band at 710–725 nm provided the best improvement. With the original 4 bands, the simulated sp. classification accuracy was 75–79%, while it was up to 85–88%, using the fifth band at the red-edge.

The aspects of utilizing reflectance anisotropy or calibrated images in high-resolution RS forest applications are largely unexplored. Studies have indicated that anisotropy might provide additional information for sp. classification (Deering et al., 1999). Line sensors offer fewer viewing directions, but owing to their view-geometry (Fig. 1), they sample the reflectance anisotropy in 1D. This may facilitate the interpretation compared to frame images. Our overall objective was to explore the ADS40 line camera for tree sp. classification of Scandinavian forests, where airborne line sensors or airborne calibrated reflectance data have not been tested thus far. Our three detailed objectives were as follows.

1. Implement an ADS40 sensor model.
2. Develop a method by which Sun-lit, shaded, camera-visible, and occluded parts of crowns can be determined to enable an extraction of image features in different illumination classes (Korpela, 2004; Larsen, 2007).
3. Examine the anisotropy and variation of spectral image features in radiometrically corrected images to study the performance potential of these data for tree species discrimination..

2. MATERIALS AND METHODS

2.1 Study area and reference trees

The experiments were carried out in Hyytiälä, southern Finland (61°50'N, 24°20'E). The study area extends 2 × 6 km and comprises protected and commercial forests. We used reference trees measured in 2005−2009 in 121, 0.04−1.8-ha plots. The age of trees was 15–150 years, and a total of 15687 reference trees were formed by image- or LiDAR-visible trees (visual interpretation). Merely 3.8% of the trees had a relative height of below 0.5. Tree maps were used to derive a proximity class for each tree, which describes the dominant species among the adjacent trees.

2.2 ADS40–SH52 and LiDAR data

The ADS40 flight was carried out on August 23, 2008 at 10–12 local time (7–9 GMT) in 15 strips. Solar elevation was 27°–37° and there were few clouds during the campaign at 700 m agl. Reflectance targets and *in-situ* radiometric measurements were carried out simultaneously. The strips were flown at 1, 2, 3, and 4 km altitudes and multispectral data was recorded for the nadir (N00A) and backward (B16A) view directions. At 1 and 2 km only N00A or B16A view was active. Strips were flown mostly in S–N direction, but also in E–W. We used discrete-return LiDAR data from 2006-2008 for the tasks of tree crown modelling and occlusion determination (section 2.6).

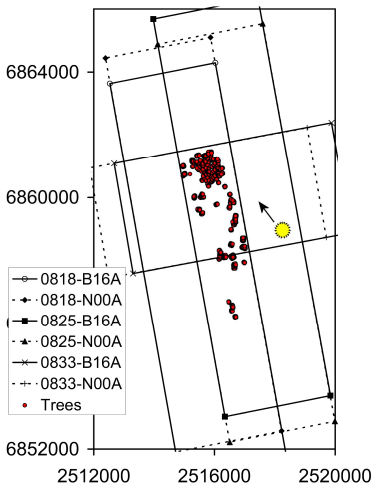

Figure 2. Footprints of 3 km strips 0818, 0825, and 0833.

2.3 Geometric and radiometric post processing of the ADS40 data

Direct georeferencing was used in aerial triangulation with 59 control points and sub-pixel accuracy was reached. Leica XPro (4.2) was used for producing three radiometrically corrected versions of each MS image:

- at-sensor radiance data ("calibrated" option): ASR
- atmospherically corrected target reflectance data ("atmospheric" option): ATM
- atmospherically and BRDF-corrected data ("atmospheric + BRDF" option): FULL

All three were produced for the 2–4 km strips, while ASR and ATM for the 1 km data. The atmospheric correction and reflectance calibration in XPro is based on the radiative transfer equation by Fraser et al. (1992). This atmospheric correction results in images, where the digital numbers are calibrated to ground reflectance. BRDF correction is based on a modified Walthall model. The details of the correction methods are presented in (Beisl et al., 2008). All corrections rely on a priori camera calibration and parameters derived from the image data. We used the default software settings in XPro processing.

2.4 Radiometric *in-situ* measurements and quality assessment of the ADS40 images

Ground measurements of reflectance targets were carried out during the overflight. Targets included reflectance tarps with 5%, 20%, 30%, and 50% nominal reflectance and well-defined surfaces (fine sand, grass, asphalt, gravel, hay). The ATM images were validated by Markelin et al. (2010) for the nadir reflectance. We sampled the targets by 4 × 4 –m rectangles and pixel data were analyzed for precision.

2.5 Photogrammetric operations in the ADS40 data

We implemented an ADS40 sensor model into the digital photogrammetric workstation KUVAMITT, guided by source-code samples from Leica. All analyses were done in epipolar images, where the distortions due to the camera movements are removed. In ADS40, the exterior orientation parameters are needed for each scanline. These were defined in a local XYZ system, which had a 3D offset and rotation with respect to the WGS84. We used accurate transformations to reach the coordinate system of the trees. Each CCD line had the xy(z) camera coordinates of the 12 000 pixels. The mapping from 3D to image was solved by iteration that limits a range of scanlines for a final sequential search of the pixel position. We used a nearest pixel interpolation.

2.6 Extraction of image features for the reference trees

We collected the image data for a reference tree by first estimating a crown envelope using LiDAR data. The crown was systematically sampled in 121 surface points, which were projected to the images. Parallel to this, each point was determined if it was visible to the camera or occluded by the tree itself or by an adjacent tree (Fig. 3). In addition, an illumination class was determined for each point using the LiDAR data in the vicinity. Accurate crown envelopes were a prerequisite. The model for crown radius was

$$r = a^2 + b \cdot h \cdot \left(\frac{5}{2}x\right)^c , \qquad (1)$$

where r is the crown radius at the relative distance $x \in (0, 0.4)$ down from the treetop. The initial values of the unknowns were set using field measurements of tree dimensions and weighted least squares adjustment with additional observation equations for a and c (to constrain their values) was used for the solution. The mean RMSE of r was 0.35 m in 15627 trees. All envelopes were convex with $c \in (0.01, 0.93)$.

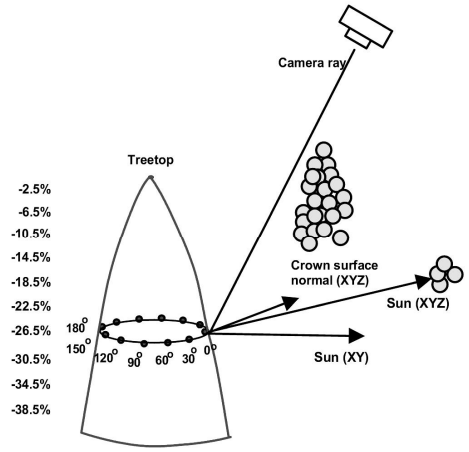

Figure 3. Determination of camera-visibility and illumination class for the 121 crown points. Each tree had 10 layers of points, and the 12 points in each had a 30° azimuth offset between points. The first point was always aligned in the direction of the solar azimuth. Two rays were cast – one towards the camera and another towards the Sun. LiDAR points were treated as 0.7-m-wide spheres (grey circles) and tested for intersection. The vector angles between the crown surface normal and the two rays defined the self-occlusion and self-shading. The example shows a camera-visible, neighbor-shaded point.

The acquisition of pixel data was repeated for the 15627 trees in 54 MS images representing different strips (15), radiometric corrections (2 or 3 per strip), and view configurations (1 or 2). Cloud screening was done in XY polygons of clouds and shadows. Crowns were sampled in 121 crown surface points (Fig. 3) that were at different relative heights symmetrically around

the crown envelope. We did not strive for complete pixel lists or image patches per tree, but samples of them.

A total of 158 features were derived for each tree, using the pixel data of the camera-visible crown points. Crown surface points belonged to an illumination class: Sun-lit (SL), self-shaded (SS), neighbour-shaded (NS), and neighbour-and-self-shaded (BS). Because of the viewing geometry and the peaked shape of the crowns, several points often mapped to the same pixel. Duplicates were filtered. The features for each tree and illumination class and the RED, GRN, BLU, NIR, and NDVI bands were: *min*, *max*, *mean*, *sdev*, and quartiles *q1*–*q3*. The topmost and lowest SL pixels were stored as separate features and band ratios were also computed.

2.7 Variables describing the view-illumination geometry

To describe the view-illumination geometry we used the *phaseangle*, *azimdiff,* and *offNadir* angles. *Phaseangle*, [0°, 180°] is the vector-angle of the camera and Sun vectors. *Azimdiff*, [0°, 180°] is the azimuth difference of the camera and Sun vectors and it is 0° for perfectly front-lit trees and 180° for back-lit trees. *OffNadir* was the angle between the plumb line and the camera vector. Fig. 4 illustrates the sampling of the view-illumination geometry.

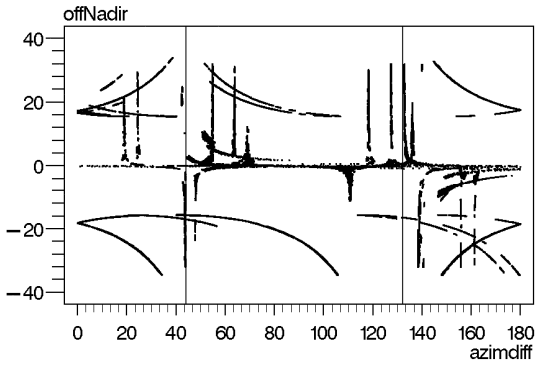

Figure 1. Distribution of *azimdiff* × *offNadir* observations (N = 202136) for all trees in all 19 strips/views. Division between front-, side-, and back-lit trees in *azimdiff* is shown by the vertical lines.

2.8 Statistical tools and classification methods

We used analyses of variance and covariance (ANOVA, ANCOVA). Classification trials were done with the quadratic discriminant analysis (QDA) with equal prior probabilities. Overall classification accuracy and the simple Kappa were the performance measures.

3. EXPERIMENTS

3.1 Evaluation of radiometric corrections and reflectance anisotopy in trees

Atmospheric effects, the changing solar elevation and the reflectance anisotropy of trees influence the pixel values in ASR images. Ideally, only the variation due to the reflectance anisotropy remains in the ATM images. In the FULL data, which combines a BRDF-correction with the ATM correction, the reflectances should be corrected also for a general anisotropy.

We first examined the ATM and FULL corrections for the coefficient of variation (CV = *sdev* / *mean*) of the intraspecies reflectance. The effects of the ATM and FULL corrections in CV were strongest in the BLU band, where the relative CVs ranged from –50% to +59% (compared to ASR data). In all bands, the effects were strongest in strips that were flown perpendicular to Sun. The FULL correction did not completely correct for the anisotropy (Fig. 5) although it produced images that are well-suited for seamless mosaicking.

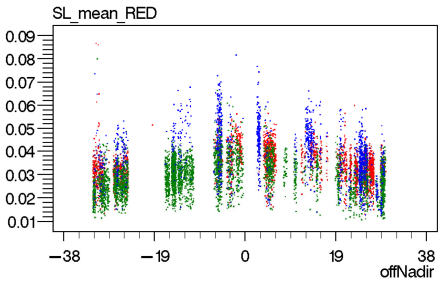

Figure 5. Scatterplot of averaged Sun-lit image data from the RED (strip 0833/N00A) band and the *offNadir* angle. FULL data. Strip 0833 was flown almost perpendicular to the Sun, where the BRDF effects are strong. Red = pine, green = spruce, blue = birch.

We also compared 1–4 km strips from different flying altitudes. The mean SL ATM reflectances per species varied up to 38% and the differences were explained by the changes in the view-illumination geometry between strips. In diffuse light, the relative differences were smaller. In well-defined targets, for the same strips, the differences were less than 10%. In two overlapping 1 km strips having a 22-minute temporal mismatch, the mean reflectances by tree species varied 2–15% depending on the band and species. The well-defined targets in these strips showed reflectance differences of below 2%. In an analysis that combined 15 strip×view combinations, the well-defined targets showed standard deviations of less than 8% for the relative differences. When restricting to reflectance tarps only, the *sdevs* were less than 6%. The results show that for well-defined targets, the precision in the ATM data was high, while the differences observed in trees were mostly due to strong reflectance anisotropy and to the naturally higher variation.

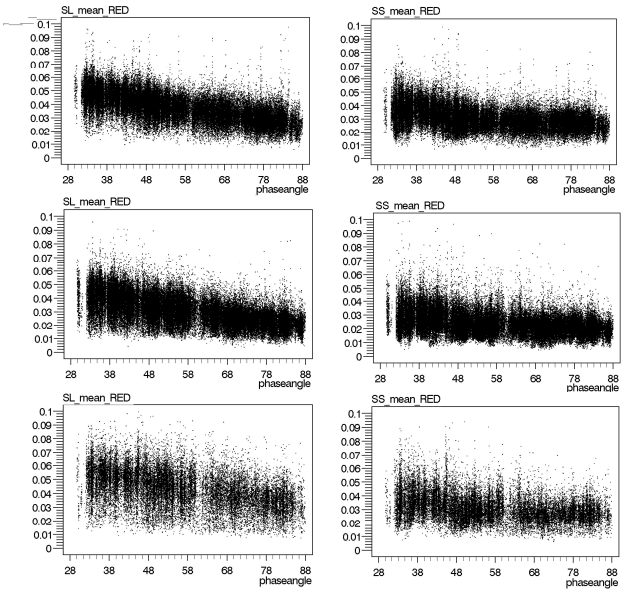

Figure 6. Distribution of RED SL (left) and SS (right) ATM reflectances (0–0.1) and the *phaseangle* (28°–88°). All 19 strips/views. Pine (top, N=80073), spruce (middle, N=93415), and birch (bottom, N=28648).

For the analysis of anisotropy, we combined the ATM data in the 19 strip/views giving over 200 000 observations. Figure 6 shows the anisotropy in ATM data (RED band) as a function of the *phaseangle*. The high intraspecies variation (CVs 12–38% over all band and species) is also obvious from Figure 6 as well as the small intraspecies differences in the mean reflectance. In diffuse light, there was no trend in high values of *phaseangle* i.e. for the back-lit trees. The anisotropy was stronger in visible bands compared to NIR (with high reflectance). Also, pine and spruce seemed to differ from birch. We tested if strongly back-lit trees would show high maximal reflectances due to forward scattering (of foliage). Such phenomenon was not observed.

3.2 Inter- and intratree reflectance variation

We studied proximity effects i.e. the influence of the immediate neighborhood to the observed reflectance. The effects were considerable in the NIR band, where adjacent birch trees caused an effect up to +33%. In the visible bands the effects were within ±10% being stronger in the diffuse light conditions.

In ANCOVA, reflectance variation was explained by *phase-angle*, *azimdiff*, *phaseangle×azimdiff*, the *strip/view* class (N = 19) variables, and age or siteindex (class). The models were fitted to the combined ATM data of all 19 strips/views. The results showed that 1–4% of the variation was contributed by the age of the trees with strongest effect in NIR and birch. The siteindex explained 1–3% of the NIR and RED band reflectances. When the stand was used as explanatory class variable, 1–19% of the reflectance variation could be contributed to the stand effect, with strongest effects in NIR in all species.

Strip/view	BAND	SL	SS	NS	BS
0825/ B16A, front-lit trees	BLU	1	0.92	0.87	0.84
	GRN	1	0.75	0.67	0.59
	RED	1	0.73	0.66	0.57
	NIR	1	0.70	0.62	0.51
0818/ B16A, back-lit trees	BLU	1	0.96	0.90	0.87
	GRN	1	0.89	0.71	0.63
	RED	1	0.92	0.72	0.64
	NIR	1	0.85	0.63	0.51

Table 1. Relative mean ATM reflectances in illumination classes (all species combined) in 3 km N-S oriented strips 0818 and 0825.

Offset to Sun	Species	BLU	GRN	RED	NIR
0°	pine	1	1	1	1
30°	"	0.99	0.98	0.97	0.97
60°	"	0.97	0.92	0.90	0.91
90°	"	0.94	0.84	0.81	0.83
0°	spruce	1	1	1	1
30°	"	0.98	0.95	0.95	0.96
60°	"	0.95	0.85	0.84	0.84
90°	"	0.91	0.75	0.73	0.73
0°	birch	1	1	1	1
30°	"	0.99	0.96	0.96	0.95
60°	"	0.95	0.87	0.87	0.85
90°	"	0.92	0.77	0.77	0.75

Table 2. Relative mean reflectances of crown points in the SL illumination class with varying solar azimuth offset. Strip 0825/B16A and ATM data with front-lit trees. Values are normalized to the 0° azimuth offset class

Intracrown reflectance variation was examined using the crown point data per tree. Table 1 shows the mean values of ATM reflectances in the for illumination classes for front- and back-lit trees. Table 2 shows the effect due to solar azimuth offset. The determination of the illumination classes succeeded based on data in Table 1, where the order of brightness was SL > SS > NS > BS. The relative difference of SL and SS was not preserved for front- and backlit trees. Table 2 shows how the brightest pixels are found in crown points that are towards the Sun and how the effect is smallest in BLU.

3.3 Feature selection and tree species classification trials

We confined to a suboptimal manual feature selection, which combined ANOVA and correlation analysis. Seven features for the classifications were: *SL_sdev_GRN*, *SL_q3_RED*, *SS_mean_BLU*, *SL_q3_NIR*, *SL_q3_NDVI*, *SL_sdev_NIR*, and *SL_mean_BLU*. The BLU band was a strong predictor, which calls into question the severity of the possible imprecision in the atmospheric correction of the BLU band (Section 3.1). Monoscopic nadir data was used with 3 and 4 km strips. The classification accuracies by strip were 72–80% (κ = 0.56–0.67) with ASR (73–80%) and ATM (75–80%) producing higher accuracies than FULL (72–78%). Accuracy varied between strips and was lower in the E–W oriented strips (72–76%) compared to the N-S strips (75–80%). Leave-tree-out and leave-plot-out validation methods produced similar accuracies as well as teaching the QDA-model with randomly selected subsets of 3×300 trees per species, which was 5–10% of the number of trees in the validation data set. Pine was classified most accurately (83–85%) in the N–S strips, with spruce at 73–76% and birch at 76–79%. In a trial, where 182982 observations in the 1–4 km ATM data were combined, the accuracy was only 62% in leave-one-out cross-validation. By restricting to three 3 km N00A views, accuracy was 72%. These results show how the anisotropy hampers classification if the view-illumination geometry is not restricted to the use of single N00A strips. When the N–S oriented strip 0825 was used for teaching and the E–W oriented strips 0843 and 0852 were used for validation, the accuracies were 54% and 68%, which demonstrates the findings of Section 3.1.

4. DISCUSSION

4.1 Confines

The presence of clouds may have affected the results. Also the timing, August 23, was quite late. The number of trees was very high. However, trees younger than 25 years were mostly missing as well as dominated trees, which remain unseen. The number of plots (121) overestimated the number of stands, because of the large size of regeneration areas in Hyytiälä.

4.2 Aim I - Sensor model implementation

We needed to implement the sensor model to do this research. However, this is a technical problem and many modern commercial digital photogrammetric workstations have the ADS40 sensor model implemented allowing standard photogrammetric procedures and workflows.

4.3 Aim II - Crown modelling and determination of illumination classes

We improved an existing method for crown modelling in LiDAR data by imposing constraints on the parameters, which enhanced the solvability of the non-linear regression. We manu-

ally positioned the treetops using photogrammetric techniques (instead of automatic tree detection) and used field measurements (instead of LiDAR measurements) to define the initial approximation of the crown envelope to be fitted in the LiDAR data. The RMSE of 0.35 m for radius suggested that the crown models were rather accurate. However, the XY position of the crown model certainly had small offsets due to measurement errors. Since real crowns are seldom rotationally symmetric, it is evident that the models were imprecise. Thus, when the crown model was sampled in surface points, some points mapped to a pixel belonging to a neighbouring tree or background. These should result in random noise. We cannot, however, exclude possible systematic errors. The ray-tracing based determination of shading and occlusion by neighbours, where LiDAR points were interpreted as opaque spheres, worked satisfactorily based on the analysis of the different illumination classes. Visual examination confirmed that the class was mostly correctly resolved. The division of canopy points between direct and diffuse light is an ill-posed task, since real crowns are semi-transparent, fractal objects.

4.4 Aim III: Evaluation of the ADS40 line sensor data for tree species classification

The ATM and FULL corrections worked well within the limits of the underlying models. The atmospheric correction was validated with well-defined targets that show only small BRDF effects. The results suggest that the precision of the ATM data was better than 10%, with NIR being the most precise and BLU the least precise. The analysis with the ATM data, where nadir views from different flying altitudes were compared, showed that the mean reflectances by species could vary −7%–+38%, depending on the band. The results showed that trees are sensitive to changes in the view-illumination geometry, which resulted in effects larger than the reflectance differences between species. The sp. classification trials demonstrated that the ATM and FULL corrections did not improve the classification performance. One reason is that the standard atmospheric correction theory does not treat shadow pixels correctly. In ANCOVA, 62−79% of the total SL reflectance variation in the BLU band of the ATM data that combined all strips and views was explained by a model that had *azimdiff*, *phaseangle*, *azimdiff×phaseangle*, and the *strip/view* class variables. In NIR, only 15−18% of the variation was explained by the same model, and the R^2 were higher in pine and spruce compared to birch. The results suggest that the anisotropy varies between species, and is strongest in the visible bands. A single BRDF-normalization for pine, spruce, and birch will likely fail. The BLU band features were strong predictors of the species. The proximity effects detected here differ from classical atmospheric scattering induced adjacency effects. To the best of our knowledge, this was the first study to show these effects, which affected the mean reflectance 1−17% in VIS bands and up to 33% in NIR. Effects by tree age and siteindex explained less than 5% of the reflectance variation with the strongest influence in NIR. Plot effect explained 1−19% of the reflectance variation and the effects were again strongest in NIR. The results of intracrown reflectance variation showed that the trends in the mean reflectances of crowns can be traced to intracrown variation, which could be used in improving the feature extraction. The 3 and 4 km nadir data showed best-case classification accuracies of 80%, which are higher than those simulated in Heikkinen et al. (2010). The fact that the reference trees were scattered across a large area and classified as a whole (vs. stand or image frame), resembling to a real forest inventory setup, is very important practical aspect, and illustrates that ADS40 in general could be very cost-efficient for tree species recognition to complement LiDAR data.

4.5 Suggestions for future research

The results in intracrown variation suggest that a different sampling strategy or weighting of the crown pixels might improve the features. The anisotropy was similar in pine and spruce, suggesting that an anisotropy correction would normalize the reflectances. Otherwise, in noisy data with high intraclass variation and small interspecies differences, the enhanced species recognition algorithm should measure the anisotropy in multiple views and use it to predict the species. This could be possible in frame images having high overlaps. It will be interesting to compare the performance of the ADS40 with other cameras in sp. classification and to complement the image features with LiDAR data to evaluate the combined performance. Also, we did not combine the two CCD views in ADS40. Heikkinen et al. (2010) suggested increasing the number of bands to five and reducing their spectral width in ADS40.

5. REFERENCES

Beisl, U., Telaar, J., Schönermark, M. V., 2008. Atmospheric correction, reflectance calibration and BRDF correction for ADS40 image data. IAPRS, Beijing, Vol. 37, part B7, pp. 7–12.

Deering, D.W., Eck, T.F., Banerjee, B., 1999. Characterization of the reflectance anisotropy of three boreal forest canopies in spring-summer. Rem Sens Env 67 (2), pp. 205–229.

Fraser, R. S., Ferrare, R. A., Kaufman, Y. J., Markham, B. L., Mattoo, S., 1992. Algorithm for atmospheric corrections of aircraft and satellite imagery. Int J Rem Sens 13 (3), pp. 541–557.

Holmgren, J., Persson, Å., Söderman, U., 2008. Species identification of individual trees by combining high resolution LiDAR data with multi-spectral images. Int J Rem Sens 29 (5), pp. 1537−1552.

Heikkinen, V., Tokola, T., Parkkinen, J., Korpela, I., Jääskeläinen, T., 2010. Simulated Multispectral Imagery for Tree Species Classification Using Support Vector Machines. IEEE Transactions Geos Rem Sens 48 (3), pp. 1355-1364.

Korpela, I., 2004. Individual tree measurements by means of digital aerial photogrammetry. Silva Fennica Monographs 3, pp. 1–93.

Larsen M., 2007. Single tree species classification with a hypothetical multi-spectral satellite. Rem Sens Env 110 (4), pp. 523–532.

Li, X., Strahler, A. H., 1986. Geometric-optical bi-directional reflectance modeling of a coniferous forest canopy. IEEE Transactions Geos Rem Sens 24, pp. 281–293.

Markelin,L., Honkavaara, E., Beisl, U., Korpela, I., 2010. Validation of the radiometric processing chain of the Leica airborne photogrammetric sensor. ISPRS Vienna 2010.

Martonchik, J.V., Bruegge, C.J. , Strahler, A.H., 2000. A review of reflectance nomenclature used in remote sensing. Remote Sensing Review 19, pp. 9–20.